Spanwise Cambered Delta Wing with Leading-Edge Separation

Joe Fernandez* and V. S. Holla†
Indian Institute of Science, Bangalore, India

Smith's method of calculating flow with leading separation on plane delta wings in subsonic flow is extended to the case of spanwise cambered delta wings, through the use of a system of conformal transformations. A numerical procedure to develop the required transformation is described. Using the transformations, a study of the effect of spanwise camber on the flow characteristics such as vortex core location and strength, sheet shape, pressure distribution, and normal force is made on a conically cambered delta wing. It is found that, at a given incidence measured from the respective zero lift angle, the core vortex on the cambered wing lies more outboard towards the leading edge and closer to the wing surface than that on the plane wing. Core and sheet vortex strengths of the cambered wing are less than those of plane wings. Significant changes in sheet shape and the location and magnitude of suction peaks are observed as a function of spanwise camber. However, with increase in incidence, the camber wing characteristics approach those of the plane wing, indicating the diminishing influence of spanwise camber on the flow details at large incidence. Since the theoretical flow model is based on the assumption of conical flow in the separated flowfield and slender wing theory for attached flow, the method is applicable in the forward region near the apex of low aspect ratio wings.

Nomenclature

A_{ij} = coefficients of orthogonal polynomial $A_i(G)$ in Eq. (9)
B_{ij} = coefficients of orthonormal polynomial $B_i(G)$ in Eq. (10)
C_k = complex constant defined in Eq. (16)
C_p = coefficient of pressure
C_{N1}, C_{N2}, C_N = linear, nonlinear, and total normal force coefficients
C_L, C_{D_i} = lift and induced drag coefficients from attached flow theory
G,H = complex variables in G and H plane, respectively
$H(G)$ = transformation function defined in Eq. (14)
I_{ik} = the integral, $\int_C G^{i-1}\bar{G}^{k-1}ds$
K_p = lift curve slope of the wing from attached flow theory $= dC_L/d\alpha$
K_i = dC_{D_i}/dC_L^2 from attached flow theory
j = distance from the vortex core to the outer end of the jth sheet segment, Fig. 4
r = polar coordinate in physical crossflow plane, Fig. 1b
s = $x \tan\delta$, the local semispan of the wing at a chordwise station x
U = freestream velocity
$W(z)$ = complex velocity potential
x,y,z = Cartesian coordinates, Fig. 1a
$z(y)$ = ordinates of the wing section measured from the plane through the wing leading edges
Z,Z^* = complex variable in Z and Z^* planes, Figs. 2a and 2d
α_G = geometric incidence, the angle between the freestream direction and the plane through the wing leading edges
$\alpha_{Z.L.}$ = zero lift angle of the wing calculated from attached flow theory
α = wing incidence measured from the zero lift angle
Γv = circulation due to vortex core
Γj = circulation of the jth sheet segment vortex
Γs = total sheet circulation
δ = semiapex angle of delta wing
θ_j = angular coordinate of jth sheet segment, measured from the line joining Z^*_v to the origin in Z^* plane, Fig. 4
ϕ = angle between radius vector r and tangent at any point on the curve, Fig. 1b
Φ = $\Phi_a + \Phi_v$
Φ_a = the sum of the velocity potential due to freestream crossflow $U\alpha$ and the attached flow perturbation velocity
Φ_v = the velocity potential due to vortex singularity distribution
$(\ )_n$ = $\partial/\partial n$ the differential in the direction of the positive normal direction
σ = arc length of the wing or sheet in crossflow plane

Received July 30, 1975; revision received May 5, 1976.
Index categories: Aircraft Aerodynamics (including Component Aerodynamics); Jets, Wakes, and Viscid-Inviscid Flow Interactions.

*Research student, Department of Aeronautical Engineering. Presently at Pennsylvania State University, State College, Pa.
†Assistant Professor, Department of Aeronautical Engineering.

Introduction

THE slender delta wing with flow separation from leading edges has been the subject of extensive theoretical and experimental studies in recent years. Quite a few methods based on different theoretical flow models have been developed.[1-4] Of these, the method of Smith[3] gives detailed information about vortex core, rolled up vortex sheet, spanwise pressure distribution, and the normal force on a plane delta wing. Polhamus'[4] method, based on leading-edge suction analogy, predicts the nonlinear part of the normal force quite accurately, but does not give any information about the details of the flow. Smith[7] has extended his method to the case of thick delta wings, and Levinsky and Wei[10] have applied it to the study of axisymmetric bodies with strakes attached.

In general, to apply Smith's method[3] to arbitrary wing or wing body combinations, one should get a conformal mapping function to transform the configuration shape in the physical crossflow plane to a vertical slit in an auxiliary plane

in which the rest of the calculations can be made using Smith's[3] theory. Except in special cases like those in Refs. 7, 10, and 11, it is difficult to get a closed-form transformation function and one has to resort to numerical methods. In the present study, a numerical procedure is developed to transform a given arbitrary closed or open curve representing the wing in the physical crossflow plane to a vertical slit in the transformed plane. The procedure, being quite general, can be used for thick or thin wings with or without being attached to a body. In this paper, the aforementioned procedure together with Smith's[3] method has been used to study the flow characteristics of a simple conically cambered delta wing of small camber with leading-edge separation. A family of such conically cambered wings with subsonic leading edges in supersonic flow have been studied by Holla and Krishnaswamy.[12] It was shown that, such wings, even without the beneficial effects of leading suction to reduce lift-dependent drag, have lift-to-drag ratios comparable to that of plane wings with suction. Further, in another study[13] it was found that minimum-drag wing shapes with conical camber and having no leading-edge suction are similar to the one considered in the present study. Further, a preliminary flow visualization experimental study in subsonic flow has shown that, on the cambered wing the vortex core, the separated sheet, and the line of reattachment were more outboard and nearer to the leading edge when compared to that of a plane wing. On the basis of these results, it was thought worthwhile to study in more detail the effect of spanwise conical camber on the flow characterisitics such as vortex core, sheet shape, and the spanwise pressure distribution. In what follows, we describe the procedure to obtain the transformation function and use it to study the effect of spanwise camber on the flow characteristics as compared to that of a plane wing. Since the theoretical flow model and calculation procedure to get flow details are essentially those of Smith the reader is referred to Ref. 3 for further details in this regard.

Smith's Flow Model

As shown in Fig. 1a, the separated shear layer from the leading edges rolls up into a concentrated vortex core standing at a distance inboard and above the wing surface. The trace of the wing with vortex core and sheet in the cross flow plane is shown in Fig. 1b. In Smith's model the separated shear layer

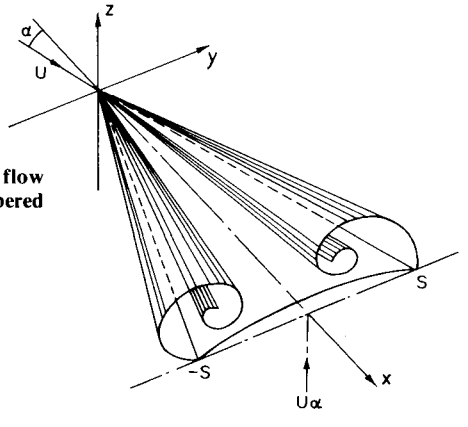

Fig. 1a Separated flow on a conically cambered delta wing.

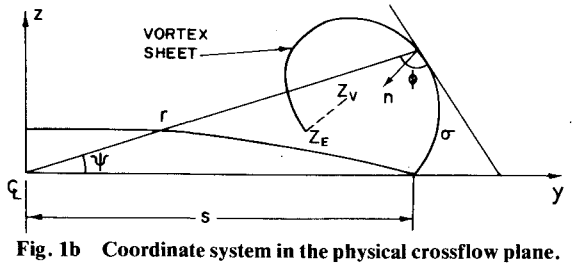

Fig. 1b Coordinate system in the physical crossflow plane.

is divided into an inner part consisting of a potential core vortex and a cut which joins the core to the free end of the outer part of the shear layer starting from the leading edge. The outer part also is represented by a distribution of potential vortices the strength of which is equal to the angular derivative of the circulation at any point along the sheet. The shape of the sheet is determined in terms of polar distances from the isolated vortex core. Using conical flow approximation to represent the flow due to separation and slender wing theory for attached flow calculations, the problem reduces to finding the velocity potential of the complete flowfield satisfying the two-dimensional Laplace equation in the physical crossflow plane. In the crossflow plane we can define a complex potential $W(Z)$ whose real part is the combined velocity potential due to crossflow stream and perturbation velocities. The velocity potential in the crossflow plane also should satisfy the following boundary conditions: 1) the Kutta-Jowkowski condition of finite velocity at the leading edge, usually called the smooth outflow condition, 2) zero total force condition on the isolated vortex and the cut so that the vortex cut system is stable, 3) the zero pressure difference condition along the sheet across which the pressure is continuous, 4) since the wing and vortex sheets are streams surfaces, the normal velocity condition on these two surfaces should be satisfied, and 5) far away from the wing the perturbation velocities due to wing and separated shear layer should vanish.

Boundary Condition on the Cambered Wing

For conical three-dimensional stream surfaces $S=S(x,r,\Psi)=0$, (which in the present case represents either the wing or the separated vortex sheet, Fig. 1b). Using the zero normal velocity condition, one can show[3] that Φ_n, the velocity normal to the trace of $S=0$, in $x=$constant crossflow plane, satisfies the relation

$$\Phi_n/U\tan\delta = -(r/s)\sin\phi \tag{1}$$

In Eq. (1), Φ is the sum of Φ_a, the attached flow potential due to wing in crossflow, and Φ_v, the perturbation potential due to vorticity distribution representing the separated sheet and rolled up vortex core. Since the wing is a stream surface even in attached flow, Φ_a should satisfy Eq. (1) together with the condition at infinity. The attached flow solution for the cambered wing can be obtained using slender body theory or any other attached flow theories. However, for wings of small spanwise camber, we use the plane wing attached flow potential at an incidence equal to that measured from the zero lift angle of the cambered wing. In doing so we are satisfying only approximately the normal velocity condition on the cambered wing for the attached flow case. Such a procedure is in order, since on the cambered wings of small camber $\sin\phi \ll 1$, so that the approximate condition on the wing for the attached flow potential can be written as

$$(\Phi_a)_n/U\tan\delta \simeq 0 \tag{2}$$

which is nothing but the exact plane wing boundary condition in attached flow.

Next, we must obtain the potential Φ_v due to distribution of vortex singularities representing the separated shear layer such that the conditions on the normal velocity on the wing and velocity at infinity, already satisfied by the attached flow potential, remain unaltered. To do this, it is convenient to transform the wing shape to a vertical slit in an auxiliary plane (Fig. 3) wherein the wing surface becomes a line of symmetry for the vortex singularity distributions and the flow tangency condition on the wing is satisfied by the principle of images. Subsequent calculations to find Φ satisfying all of the conditions listed earlier are made in the transformed plane. A numerical procedure to get the required transformation is described in the next section.

Conformal Mapping

For wings of arbitrary shape, with open or closed contours in physical crossflow plane, it is not always possible to get a simple closed-form transformation function to map the wing contour to a vertical slit, except in some special cases like those in Refs. 3, 7, 10, and 11. For the general case, it is shown that the required transformation can be obtained, through a series of three successive conformal mapping functions, two of which are in closed analytical form and the remaining one obtained by numerical procedure using a set of orthonormal functions defined over a closed contour. Successive stages of transformation of the wing contour to a vertical slit are shown in Fig. 2.

First of all, the wing contour (an open or closed curve) in the physical crossflow plane, defined by

$$Z=z(y)/s \qquad -1\le y/s\le 1 \tag{3}$$

is transformed to a closed curve C in G plane using the inverse Joukowsky transformation

$$G=[Z\pm\sqrt{Z^2-1}\,] \tag{4}$$

For wings of small camber, this transformation maps the open curve onto a near circle in G plane (Fig. 2b).

The second transformation maps the region exterior to C in G plane to the exterior region of a unit circle in H plane. (Fig. 2c). The required exterior mapping is related closely to the set of complex orthonormal polynomials defined on the curve C.[5] To get these orthonormal polynomials, consider the set of analytic functions

$$1,G,G^2\ldots,G^n,\ldots \tag{5}$$

Let $A_i(G)$ ($(i=1,2,\ldots,N)$ a polynomial of degree $(i-1)$ be the ith member of a set of N orthogonal polynomials constructed using the foregoing analytic functions. The polynomials are orthogonal in the Szego[6] sense so that

$$(A_iA_j)=\int_C A_i(G)\overline{A_j(G)}\,ds$$

$$=0 \qquad i\neq j$$

$$\neq 0 \qquad i=j \tag{6}$$

where ds is the incremental arc length along C. The integral in Eq. (6) is known as the Szego inner product of two polynomials defined over C and is denoted as (A_iA_j). The norm $N(A_i)$ of each orthogonal polynomial is defined as

$$N(A_i)=\left\{\int_C |A_i(G)|^2 ds\right\}^{1/2} \tag{7}$$

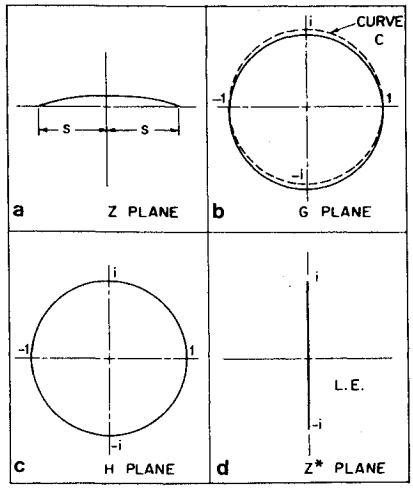

Fig. 2 Changes under the successive transformations for a simple cambered wing.

and the ith orthonormal function $B_i(G)$ is given by

$$B_i(G)=A_i(G)/N(A_i) \tag{8}$$

Using the well-known Gram-Schmidt orthogonalization procedure starting with unity as the first orthogonal function, we obtain the ith orthogonal function of $A_i(G)$ as a linear combination of G^{i-1} and all of the previous $(i-1)$ orthonormal functions such thet $A_i(G)$ is orthogonal to all $A_j(G)$ $(j=1,2,\ldots,i-1)$. In general, we can write

$$A_i(G)=A_{i,i}G^{i-1}+A_{i,i-1}B_{i-1}+\ldots+A_{i,1}B_1 \tag{9}$$

and the corresponding orthonormal function as

$$B_i(G)=B_{ii}G^{i-1}+B_{i,i-1}G^{i-2}+\ldots+B_{i,1} \tag{10}$$

From the orthogonality conditions, one can show that $A_{i,j}$ and $B_{i,j}$ are given by the following relations.

$$A_{i,j}=-\sum_{k=1}^{j}\bar{B}_{jk}I_{i,k} \qquad \begin{matrix} i=2,3,4\ldots \\ j=1,2,\ldots,(i-1)\end{matrix} \tag{11}$$

with $A_{ii}=1$, $i=1,2,3,\ldots$.

$$B_{i,j}=\frac{1}{N(A_i)}\sum_{k=j}^{i-1}A_{i,k}B_{k,j} \qquad \begin{matrix} i=2,3,4,\ldots \\ j=1,2,\ldots,(i-1)\end{matrix} \tag{12}$$

with $B_{ii}=1/N(A_i)$, $i-1,2,\ldots$.The $I_{i,k}$ defined in Eq. (11) are the inner products of powers of G and are defined as

$$I_{i,k}=(G^{i-1},G^{k-1})=\int_C G^{i-1}\bar{G}^{k-1}ds \tag{13}$$

Now the required mapping function to map the exterior of the curve C in G plane to outside the region of a unit circle in H plane is given by

$$H(G)=\lim_{N\to\infty}\frac{B_{N+1}(G)}{B_{N(G)}}=\frac{\sum_{i=1}^{N+1}B_{N+1,i}G^{i-1}}{\sum_{i=1}^{N}B_{N,i}G^{i-1}} \tag{14}$$

which is nothing but the ratio of successive orthonormal polynomials with N, the order of the polynomial, being taken large for improved accuracy.

The orthonormalization scheme just described can be used for machine computation to obtain the coefficients $B_{i,j}$ by numerical methods. However, the numerical procedure becomes unstable because of inherent truncation and round-off errors, and $A_i(G)$ becomes nonorthogonal beyond a certain value of i. An iterative correction scheme of Davis and Rabinowitz[8] has been applied to improve the orthogonality of each function $A_i(G)$ as it is generated, until the convergence is obtained. From the extensive numerical studies it was found sufficient to consider polynomials of order $N+1=9$ to get a good convergent mapping function.

Finally, using the transformation

$$Z^*=\tfrac{1}{2}(H-1/H) \tag{15}$$

The region outside the unit circle is transformed to the entire z^* plane, with the unit circle itself being transformed to a vertical slit $-i\le Z^*\le i$.

Next we need the inverse transform of the three transformations described earlier, to know the flowfield details in the physical plane. Although the transformations (4) and (15) can be inverted analytically, we again have to use numerical methods to invert the transformation (14). This is done by

expanding $G=G(H)$, the inverse mapping function, in terms of a set of orthonormal functions in the region $|H|\geq 1$, as

$$G=\frac{1}{\sqrt{2\pi}}\sum_{k=1}^{M} C_k H^{(2-k)} \tag{16}$$

The constants C_k are given by the integral

$$C_k=\frac{1}{\sqrt{2\pi}}\int_{|H|=1} G\bar{H}^{(2-k)}\,ds \tag{17}$$

The real and imaginary parts of C_k are given by

$$\mathrm{Re}(C_k)=\frac{1}{\sqrt{2\pi}}\int_0^{2\pi}[X\cos(k-2)\theta - Y\sin(k-2)\theta]\,d\theta \tag{18a}$$

$$\mathrm{Im}(C_k)=\frac{1}{\sqrt{2\pi}}\int_0^{2\pi}[X\sin(k-2)\theta + Y\cos(k-2)\theta]\,d\theta \tag{18b}$$

with $s=r\theta$, $r=1$, $G(\theta)=X(\theta)+iY(\theta)$, and the values of $G(\theta)$ on the unit circle are obtained from the forward transformation $H=H(G)$. During numerical computation it was found that, even with $M=10$, the G values obtained were in error by about 5%. Hence, an approximate value of G was calculated with $M=12$ and the accuracy was improved using a complex Newton-Raphson technique. The relation

$$G_{n+1}=G_n-[H(G)-H]/H'(G) \quad n=0,1,2,\ldots \tag{19}$$

was used iteratively until the sequence G_n converged to G within a preassigned tolerance.

Numerical Calculation in Z^* Plane

Once the cambered wing is transformed to the vertical slit in Z^* plane (Fig. 3) the rest of the calculations to obtain the flow details are made using Smith's[3] procedure. The trace of the wing and the position of the isolated vortex and the vortex sheet locations are shown in Fig. 3. The vortex core is connected through a cut to the vortex sheet which is divided into segments between the cut and the wing leading edge. We have to find $(2n+2)$ unknowns which are the strengths Γ_j and locations Z^*_j of sheet vortices $(2n$ values) and the strength Γ_v and location Z^*_v of the isolated vortex core. For this we require $(2n+2)$ equations, which we obtain by satisfying the normal velocity and pressure continuity conditions at the midpoints of each segment $(2n$ equations) together with the condition of zero total force on the vortex core and the cut system and the leading edge Kutta condition. With an assumed initial set of values for the strength and locations of sheet and core vortices, the sheet strengths are determined in terms of isolated core strength using the pressure continuity condition across the sheet. To determine the core vortex strength and location, the Kutta condition at the leading edge and the zero force condition on the vortex core-cut system are used, respectively. To determine the core location, a deterministic pattern search method (because of its good convergence even with poor initial values) is used initially until the vortex core moves close to the point corresponding to the minimum modulus of force. Then we switch over to a rapidly convergent method from Warner,[9] finally fix the core location. Finally, without changing the quantities already determined as aforementioned, the sheet shape is found using the condition on the velocity normal to the sheet. These steps are carried out in nested iterative loops until convergence is obtained in each step. At the end of these calculations we get Γ_v, Z^*_v, Γ_j and Z^*_j for a given value of $\alpha/\tan\delta$. Finally, the required aerodynamic quantities i.e. linear and nonlinear parts of the normal force coefficient and spanwise pressure distributions are obtained using the relevant expressions. Here we have indicated briefly the procedure. The basic mathematical relations and the details of numerical procedure can be found in Smith's[3] original work, and also in Ref. 14.

Numerical Example: A Simple Conically Cambered Wing

Smith's[3] method together with conformal transformations discussed earlier have been applied for the case of a simple conically cambered delta wing (Table 1), to study the effect of spanwise camber on the flow characteristics. The cambered wing under consideration belongs to a family of conically cambered delta wings studied in Ref. 12. The strength and shape of the vortex sheet, core vortex strength and location, spanwise pressure distribution, and the overall normal force coefficient are calculated at different values of $\alpha/\tan\delta$ and the results are compared with those of a plane wing. The incidence α on both wings is measured from the respective zero lift angle which, for the cambered wing, has been calculated using Multhopp's lifting surface theory. After an extensive numerical study, the angular extent of the sheet was fixed at 2.75 rad and the sheet was represented by 11 segments. In general, it was found that the numerical procedure breaks down for $\alpha/\tan\delta<0.2$. However, in this range, the approximate results can be obtained by extrapolation, as can be seen from the results presented herein.

Core Vortex and Sheet Shape

The lateral and vertical locations of the vortex core on both wings at different incidences are plotted against $\alpha/\tan\delta$ in Fig. 4. With increase in incidence the vortex core moves upward

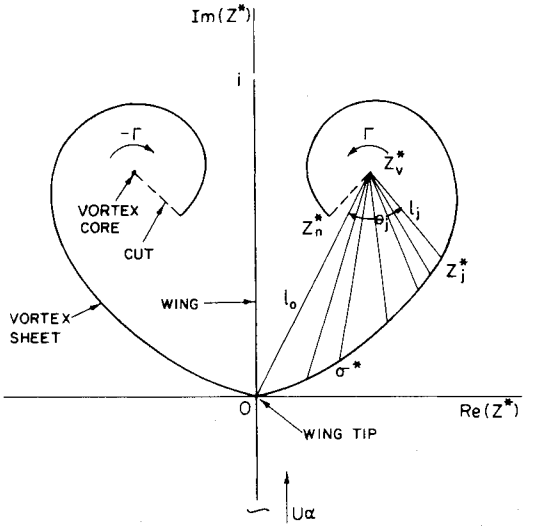

Fig. 3 Configuration in the transformed (Z^*) plane.

Table 1 Wing camber distribution

$\eta=y/x\tan\delta$	$z/x\tan\delta$
0	0.05
0.1	0.04948875
0.2	0.04795498
0.3	0.04540354
0.4	0.04183923
0.5	0.03727331
0.6	0.03171624
0.7	0.02518328
0.8	0.01769272
0.9	0.00926286
1.0	0

and inboard, on both wings. But, at any incidence, the core vortex on cambered wing is located more outboard and nearer to the wing surface than that on the plane wing. The difference between the vortex core locations on the two wings at a given incidence reduces very much with increase in incidence, thereby indicating that, at large incidence, the spanwise camber has little effect on the core location.

In Fig. 5, the vortex sheet shape on both wings is shown for $\alpha/\tan\delta = 0.3$, 0.9, and 1.5. In general, the sheet shapes are similar on both wings, with the plane wing having a larger sheet length. There is a significant difference in the sheet shape of the two wings nearer to the wing leading edge. Unlike that of the plane wing, the cambered wing sheet initially moves a little inboard of the leading edge up to a certain height and then changes its curvature and bulges outward. A similar trend also was noticed by Smith[7] and Barsby[11] in their calculations on thick wings and circular arc conically cambered wings, respectively, but at smaller values of $\alpha/\tan\delta$ only. They attributed this result to the failure of the numerical procedure at small values of $\alpha/\tan\delta$. One reason for such a behavior is that, on the cambered wing the core vortex, though of slightly lesser strength, being closer to the wing surface and the leading edge, creates a higher suction on the wing near the edge (see Fig. 6). Consequently, the separated shear layer from the leading edge is drawn inboard to an extent greater than that in the case of the plane wing. Once it is outside the region of influence of this locally high suction, the sheet bulges out before finally rolling up into the vortex core as in the case of the plane wing.

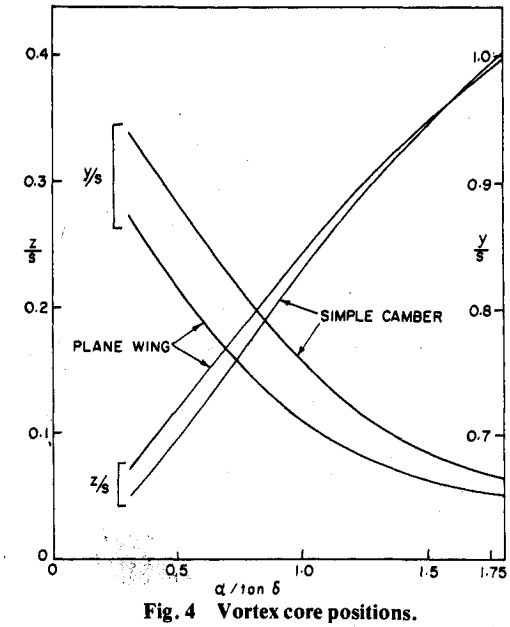

Fig. 4 Vortex core positions.

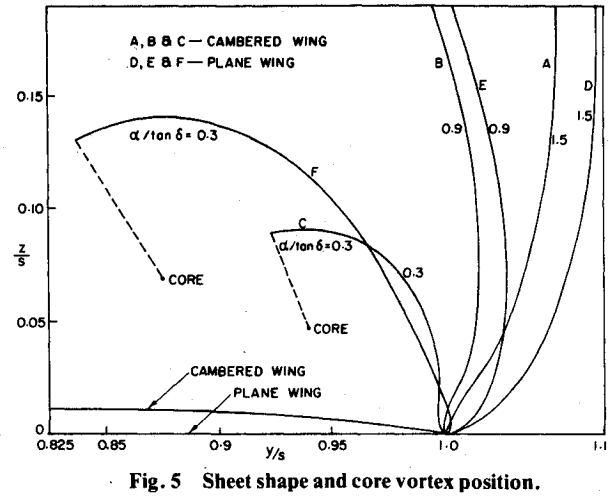

Fig. 5 Sheet shape and core vortex position.

Circulation Γ_v and Γ_s

In Table 2 the circulation due to core vortex and the total circulation of the sheet are given for $\alpha/\tan\delta$ in the range $0.3 \le \alpha/\tan\delta \le 1.8$. Although Γ_v and Γ_s of the cambered wing are less than that of the plane wing at any incidence, the ratio Γ_v/Γ_s of the cambered wing is larger than that of the plane wing. This shows that the spanwise camber has not only reduced but also effected a redistribution of the vortex strengths between the core and the sheet. Further, a simple calculation based on results in Table 2 shows that, at smaller incidences, the reduction in total circulation $(\Gamma_v + \Gamma_s)$ due to spanwise camber is a large percentage of the plane wing value, (e.g. 30% reduction at $\alpha/\tan\delta = 0.3$). With increase in incidence this percentage reduction in $(\Gamma_v + \Gamma_s)$ decreases nonlinearly with incidence (e.g. 4.13% at $\alpha/\tan\delta = 1.8$). This shows that at higher angles of attack the effect of spanwise camber is negligible in reducing the overall circulation.

Spanwise Pressure Distribution

The spanwise pressure coefficient distribtions on top and bottom surfaces of two wings for $\alpha/\tan\delta = 0.3$, 0.6, 0.9, 1.2, and 1.5 are shown in Fig. 6. The difference in C_p distribution between plane and cambered wings is negligible on the bottom surface all along the span. On the top surface, it is seen that the suction peak on the cambered wing is larger and is associated with a larger pressure gradient, in addition to being situated more outboard than that on the plane wing. With increase in incidence, on both wings, the suction peak becomes larger and occurs at more inboard stations, but the difference in magnitude and the location of the suction peak between the two wings decreases. An interesting point to note is that the spanwise location of the suction peak (Fig. 6) and the vortex core (Fig. 4) are almost identical at all incidences on both wings. Hence, from experimental pressure measurement data one can find the spanwise position of the rolled up vortex core on the wing.

Table 2 Vortex core and sheet circulation

α	Plane wing			Cambered wing		
	Γ_v	Γ_s	Γ_v	Γ_v	Γ_s	Γ_v
$\tan\delta$	*Us* $\tan\delta$	*Us* $\tan\delta$	Γ_s	*Us* $\tan\delta$	*Us* $\tan\delta$	Γ_s
0.3	1.019	0.16	6.3687	0.774	0.054	14.3333
0.4	1.371	0.261	5.2528	1.154	0.116	10.9498
0.5	1.724	0.378	4.5608	1.537	0.198	7.7626
0.6	2.081	0.506	4.1126	1.927	0.301	6.4019
0.7	2.446	0.646	3.7863	2.316	0.422	5.4881
0.8	2.822	0.792	3.5631	2.709	0.558	4.8548
0.9	3.213	0.944	3.4036	3.107	0.703	4.4196
1.0	3.619	1.095	3.3050	3.513	0.858	4.0944
1.1	4.041	1.243	3.2457	3.930	1.014	3.8795
1.2	4.482	1.397	3.2083	4.361	1.168	3.7337
1.3	4.941	1.547	3.1939	4.806	1.322	3.6354
1.4	5.419	1.694	3.1989	5.267	1.476	3.5684
1.5	5.913	1.837	3.2188	5.746	1.623	3.5403
1.6	6.425	1.977	3.2498	6.243	1.769	3.5291
1.7	6.954	2.115	3.2879	6.754	1.910	3.5361
1.8	6.498	2.248	3.3354	7.284	2.049	3.5549

Normal Force

In Table 3 the normal force coefficients on the two wings for different $\alpha/\tan\delta$ are given. Since the attached flow solution for the cambered wing is approximated to that of a plane wing at an incidence equal to that measured from the zero lift angle of the cambered wing, the linear part of the lift on the two wings is the same. The total normal force on the cambered wing varies approximately from about 0.9 to 0.96

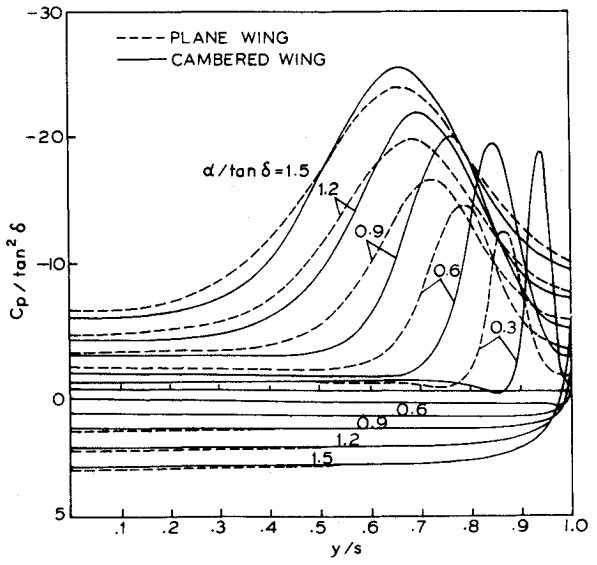

Fig. 6 C_p distribution along the semispan.

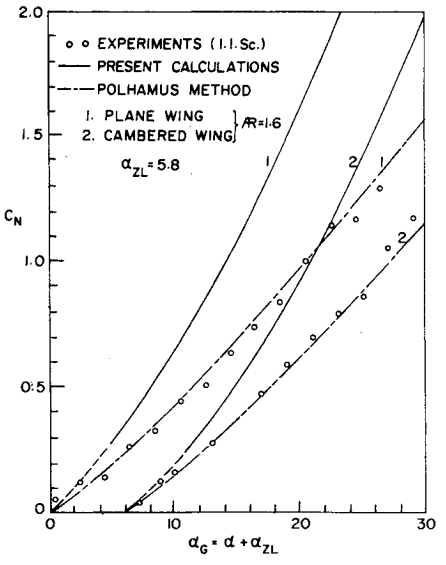

Fig. 7 Normal force on plane and cambered wings.

times the corresponding plane wing values as $\alpha/\tan\delta$ varies from 0.3 to 1.8.

In Fig. 7, the total normal force coefficients calculated from the present method are compared with the experimental results (the experiments were conducted on a plane and cambered wing, both of $AR=1.6$, in the 9 ft × 5 ft elliptic test section closed-circuit wind tunnel at the Indian Institute of Science[14]), as well as those obtained using the Polhamus[4] method. According to this method, the nonlinear part of the normal force is related to the leading-edge suction force calculated using the attached flow theory. The total normal force coefficient on a plane delta wing of sweep angle Λ is given by

$$C_N = K_p \sin\alpha\cos\alpha + K_p(1 - K_p K_i)\sin^2\alpha/\cos\Lambda \qquad (20)$$

where $K_p = dC_L/d\alpha$ and $K_i = dC_{Di}/dC_L^2$. To use this relation for the cambered wing, we identify α as the incidence measured from the attached flow zero lift angle of the cambered wing, so that $\alpha = \alpha_G - \alpha_{Z.L.}$. In doing so, we are accounting for only the leading suction force corresponding to the additional load due to increase in incidence from $\alpha_{Z.L.}$. The values of K_p and K_i and $\alpha_{Z.L.}$ are calculated using the well-known Multhopp's lifting surface theory. As seen from Fig. 7, the present method gives an overestimation of C_N, whereas Polhamus theory results agree well with experimental results. The reasons for such discrepancies are the following. Firstly, the nonexistence of the assumed conical flow conditions on the vortex sheet over the entire wing, particularly near the trailing edge, leads to an overestimation of nonlinear lift. Secondly, the slender wing theory also leads to incorrect estimation of the linear part of the normal force, since the zero load condition at the trailing edge is not satisfied. Thirdly, in the present case, the wings used for the experiment have an $AR = 1.6$ which lies outside the range of applicability of the present method, but well within the range of applicability of the Polhamus method. However, as shown by Smith[3], a good agreement between measured and estimated C_N can be obtained if one computes the C_N from experimental pressure data measured in the forward region of a low aspect ratio wing, in which case the assumed flow conditions largely prevail.

Conclusions

In the present study a procedure is developed to extend Smith's[3] method to the study of nonplanar delta wings with leading-edge separation. For this purpose a method is given to transform the arbitrary spanwise profile shape to a vertical slit by using a series of conformal transformations. The method is quite general in nature and can be used in the study of 1) nonplanar wing and body interference with and without leading-edge separation, and 2) conical thick wings with leading-edge separation. Also, with certain modification, the

Table 3 Normal force coefficients

α		$C_{N_2}/\tan^2\delta$		$C_N/\tan^2\delta$	
$\tan\delta$	$CN_1/\tan^2\delta$	Plane	Cambered	Plane	Cambered
0.3	1.885	0.617	0.373	2.502	2.258
0.4	2.513	1.018	0.707	3.532	3.221
0.5	3.141	1.496	1.128	4.638	4.270
0.6	3.769	2.048	1.637	5.818	5.407
0.7	4.398	2.673	2.224	7.071	6.622
0.8	5.021	3.365	2.884	8.392	7.911
0.9	5.655	4.122	3.611	9.777	9.266
1.0	6.283	4.937	4.402	11.220	10.685
1.1	6.911	5.810	5.244	12.722	12.155
1.2	7.539	6.738	6.139	14.278	13.679
1.3	8.168	7.717	7.083	15.886	15.252
1.4	8.796	8.747	8.075	17.544	16.872
1.5	9.425	9.826	9.112	19.251	18.536
1.6	10.053	10.951	10.189	21.003	20.043
1.7	10.681	12.620	11.312	22.060	21.993
1.8	11.309	13.334	12.470	24.643	23.784

second transformation together with the Joukowsky transformation can be used in the study of two-dimensional aerofoils, with or without camber.

The effect of spanwise camber on the flow characteristics of nonplanar delta wing with leading-edge separation is illustrated through the application of the present method to the case of a conically cambered delta wing with small spanwise camber, and the following conclusions are derived.

1) At a given incidence measured from the respective zero lift angles, the core vortex on the cambered wing lies more outboard and closer to the wing surface than that on a plane wing.

2) Because of spanwise camber, the strength of the core and sheet vortices and the nonlinear normal force are reduced.

3) Significant changes in the sheet shape are observed very near the leading edge and the magnitude and location of the suction peak is altered appreciably.

4) With increase in incidence, the cambered wing characteristics approach those of the plane wing, thereby indicating the diminishing of wing camber influence on the flow properties at large angles of attack.

Finally, the validity of the present method is restricted to the class of small aspect wings and to the regions of separated flow in the forward part nearer to wing apex, where the flowfield is to a good approximation conical. The method presented here also has been used in the study of a family of conically cambered delta wings with reflex spanwise curvature and the results are presented in a separate paper to be published elsewhere.

References

[1]Brown, C. E. and Michale, W. H., "On Slender Delta Wings with Leading Edge Separation," *Journal of the Aeornautical Sciences,* Vol. 21, Oct., 1954, pp. 690–694, 706.

[2]Mangar, K. W. and Smith J. H. B., "A Theory of Flow Past Slender Delta Wings with Leading Edge Separation," Rept. Aero-2593, Royal Aircraft Establishment, Farnborough, England, 1957; also *Proceedings of the Royal Society, London,* A. 251, May 1959, p. 200.

[3]Smith, J. H. B., "Improved Calculation of Leading Edge Separation from Slender Delta Wings," Royal Aircraft Establishment, Farnborough, England, TR 6607, March 1966; also *Proceedings of the Royal Society, London,* A 306, July 1968, p. 67.

[4]Polhamus, E. C., "A Concept of the Vortex Lift of Sharp Edge Delta Wings Based on Leading Edge Suction Analogy," NASA TND-3767, Dec. 1966.

[5]Kantorovich, L. V. and Krylov, V. I., *Approximate Methods of Higher Analysis,* P. Noordhoof Ltd., Groningen, The Netherlands, 1958, Chap. V, Sec. 4, p. 381.

[6]Szego, G. , *Orthogonal Polynomials,* American Mathematical Society Colloquium Publications, New York, 1939.

[7]Smith J. H. B., "Calculation of the Flow over Thick Conical Slender Wings with Leading Edge Separation," Royal Aircraft Establishment, Farnborough, England, TR 71057, March 1971.

[8]Davis, P. J. and Rabinowitz, P., "Advances in Orthonormalizing Computation," *Advances in Computers,* Vol. 2, Academic Press, New York, 1961.

[9]Warner, F. J., "On the Solution of Jury Problem with Many Degrees of Freedom," *Mathematical Tables and Other Aids to Computation,* National Research Council, Washington, D. C., 1957, Vol. 11, pp. 268–271.

[10]Levinsky, E. S. and Wei, M. H. Y., "Nonlinear Lift and Pressure Distribution on Slender Conical Bodies with Stakes at Low Speeds," NASA CR 1202, Oct. 1968.

[11]Barsby, J. E., "Flow Past Conically Cambered Slender Delta Wings with Leading Edge Separation," Aeronautical Research Council, London, England, R&M 3748, Sept. 1972.

[12]Holla, V. S. and Krishnaswamy, T. N., "Conically Cambered Triangular Wings," *Journal of the Aeronautical Society of India,* Vol. 22, May 1970, pp. 94–107.

[13]Holla, V. S., Krishnaswamy, T. N., and Ramchandra, S. M., "Conically Cambered Triangular Wings Optimised for Least Drag without Leading Edge Suction," Aerohautical Research Committee Council of Scientific and Industrial Research, India, Rept. No. ARCTR-2, Oct. 1971.

[14]Fernandez J., "Leading Edge Separation from Slender Delta Wings," M.Sc. Thesis, Aug. 1973, Dept. of Aeornautical Engineering, Indian Institute of Science, Bangalore, India.